Joule

CellPress
OPEN ACCESS

Article

CO_2 electroreduction to multicarbon products from carbonate capture liquid

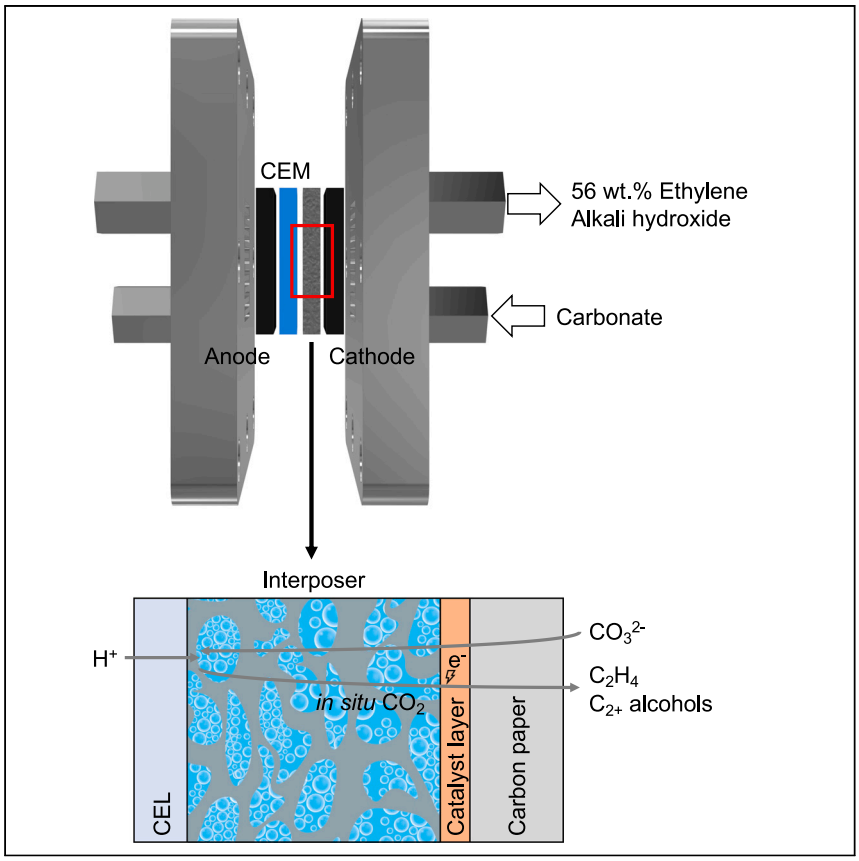

Reactive capture systems unite CO_2 capture with CO_2 upgrade/utilization into more valuable chemicals. We, herein, present the direct electrochemical upgrade of carbonate, captured CO_2 in direct air capture, into C_2 and higher products (C_{2+}). Interposer and catalyst joint design enables us to electroproduce 56 wt % C_2H_4 from a carbonate solution with no detected CO_2 in the gas stream. The carbonate electrolysis system produces a gas stream that is undiluted by CO_2 and accomplishes complete CO_2 utilization, reducing regeneration/separation costs.

Geonhui Lee, Armin Sedighian Rasouli, Byoung-Hoon Lee, ..., Zhu Chen, David Sinton, Edward Sargent

ted.sargent@northwestern.edu

Highlights

The electrochemical upgrade of CO_2 captured in the carbonate form to C_{2+} products

Studying key metrics (local pH and reactant concentration) in reactive capture

Interposer and catalyst joint design enables the electrosynthesis of 56 wt % C_2H_4

Reactive capture obviates the need for energy to regenerate lost/unreacted CO_2

Lee et al., Joule 7, 1277–1288
June 21, 2023
https://doi.org/10.1016/j.joule.2023.05.003

Joule

CellPress
OPEN ACCESS

Article

CO_2 electroreduction to multicarbon products from carbonate capture liquid

Geonhui Lee,[1,6] Armin Sedighian Rasouli,[1,6] Byoung-Hoon Lee,[1,6] Jinqiang Zhang,[1] Da Hye Won,[2] Yurou Celine Xiao,[3] Jonathan P. Edwards,[3] Mi Gyoung Lee,[1] Eui Dae Jung,[1] Fatemeh Arabyarmohammadi,[3] Hengzhou Liu,[4,5] Ivan Grigioni,[1] Jehad Abed,[1] Tartela Alkayyali,[3] Shijie Liu,[3] Ke Xie,[1] Rui Kai Miao,[3] Sungjin Park,[1] Roham Dorakhan,[1] Yong Zhao,[3] Colin P. O'Brien,[3] Zhu Chen,[1] David Sinton,[3] and Edward Sargent[1,4,5,7,*]

SUMMARY

Alkali hydroxide systems capture CO_2 as carbonate; however, generating a pure CO_2 stream requires significant energy input, typically from thermal cycling to 900°C. What is more, the subsequent valorization of gas-phase CO_2 into products presents additional energy requirements and system complexities, including managing the formation of (bi)carbonate in an electrolyte and separating unreacted CO_2 downstream. Here, we report the direct electrochemical conversion of CO_2, captured in the form of carbonate, into multicarbon (C_{2+}) products. Using an interposer and a Cu/CoPc-CNTs electrocatalyst, we achieve 47% C_{2+} Faradaic efficiency at 300 mA cm^{-2} and a full cell voltage of 4.1 V. We report 56 wt % of C_2H_4 and no detectable C_1 gas in the product gas stream: CO, CH_4, and CO_2 combined total below 0.9 wt % (0.1 vol %). This approach obviates the need for energy to regenerate lost CO_2, an issue seen in prior CO_2-to-C_{2+} reports.

INTRODUCTION

CO_2 capture from air and oceans, when combined with an upgrade into chemicals that serve as precursors to long-lived materials, offers to contribute carbon-negative (cradle-to-gate) solutions that offset difficult-to-abate emissions on the path to net-zero emissions.[1–3] Reactive capture systems unite CO_2 capture with CO_2 upgrade/utilization into more valuable chemicals. Much progress has been made electrochemically generating CO from captured CO_2, on the path to fuels and chemicals via syngas processes.[4–8] In thermochemistry, reactive capture has proceeded to methane, methanol, and formate.[9–11]

C_2 and higher products (C_{2+}) represent a large global market: ethylene and ethanol lie in the range of ~US$230B and ~US$160B, respectively,[12,13] in contrast with the C_1 chemicals (CO and formic acid) generated by reactive capture to date, whose combined values are below US$12B.[14,15] Yet, to date, it is mainly C_1 products that have been produced in reactive capture systems of both electrochemical and thermochemical types.

Direct air capture (DAC) using alkali hydroxide captures CO_2 as carbonate and generates a pure/concentrated gas-phase CO_2 stream via thermal swing at ~900°C.[16] The subsequent valorization of gas-phase CO_2 into value-added products

CONTEXT & SCALE

Cradle-to-gate carbon-negative technologies, including direct air capture (DAC), have shown promise in mitigating CO_2 emissions. However, these emerging technologies to capture CO_2 from the air rely on a thermal swing to release concentrated CO_2, and today this comes at a high energy cost. The ensuing step in gas-phase CO_2 electrolysis requires additional energy. Furthermore, this step suffers from incomplete CO_2 conversion. This leads to a high cost to regenerate/separate (otherwise-lost/unreacted) CO_2.

To tackle these challenges, a scheme known as reactive capture has been proposed: the integrated systems for capture-and-upgrade of CO_2 to valuable products. This approach is the direct conversion of chemisorbed CO_2 into value-added products. The benefits of reactive capture are (1) to avoid the energy-intensive and carbon-positive steps associated with concentrating CO_2 and (2) to enable ~0% reactant losses. This obviates the need for energy to regenerate/separate lost/unreacted reactants.

introduces further energy losses and system complexity. This approach involves introducing CO_2 in the gas phase for electrolysis.

In contradistinction, reactive capture takes the carbon source from carbonate species, bypassing CO_2 concentrating steps. In prior reports of reactive capture from carbonate, Li et al. demonstrated pure syngas production with Faradaic efficiency (FE) of ~30% CO and ~70% H_2, and with a Cu electrocatalyst, ~14% C_2 FE was observed.[5] The authors reported no appreciable loss of CO_2 during carbonate electrolysis. Such prior studies offer a path to avoid the energy-intensive steps associated with concentrating CO_2 and regenerating lost CO_2; however, until now, the selectivity toward more valuable CO_2-derived products has been limited compared with the diversity of products available in electrochemical CO_2 reduction reaction (CO_2RR) systems.

Such electrochemical CO_2RR systems, although they have achieved impressive increases in performance,[17,18] suffer—in the case of alkaline and neutral CO_2RR—from low CO_2 utilization (the fraction of input CO_2 converted into desired products) that is $\leq$25% in the case of C_2 production due to carbonate formation in locally alkaline conditions.[19] The low CO_2 utilization leads to a high cost to regenerate (otherwise-lost/emitted) CO_2.[19,20] Enticingly, recent studies have overcome this CO_2 utilization limit via local CO_2 regeneration[21–23]; however, until now, the product gas stream has still been diluted by unreacted CO_2 and gas-phase CO_2-derived products such as carbon monoxide and methane.[22,24,25] Even in systems that achieved >76% CO_2 utilization via local CO_2 regeneration, unreacted CO_2 remains >56 wt % (Table 1).

Since CO_2 separation is an energy-intensive process (2–4.4 GJ/tonne of CO_2),[16,26,27] unreacted CO_2 significantly increases overall system energy requirements. Eliminating CO_2 at the downstream could lead to a lower cost of purification demand.[20,28]

Here, we pursue C_{2+} products from carbonate solution—a liquid used in DAC—in an electrochemical reactive capture system. Among the striking results is a negligible presence (sub 1%) of CO_2 and C_1 gas products such as CO and CH_4 in the electrolyzer outlet, a finding promising for the minimization of product separation costs.

RESULTS

Modeling of carbonate electrolysis

In prior reports of reactive capture from carbonate,[5] *in situ* CO_2 is regenerated via an acid/base reaction between carbonate and protons. Protons come from the cation-exchange layer (CEL) of a bipolar membrane (BPM) under reverse bias. The *in situ* CO_2 is converted to CO_2-derived products at the surface of a Cu electrocatalyst, with C_2 (e.g., to ethylene and ethanol) selectivity totaling below 14% (Figure S1).

We used modeling of chemical species generation, consumption, and diffusion to seek an explanation of why C_{2+} productivity is low in prior reactive capture studies and to identify system architectures to increase it (Figure 1B; Notes S1 and S2). The modeling results show that the spacing between the CEL of BPM and the electrocatalyst influences species concentrations in the reactive capture system (Figures S2–S6). The concentrations of CO_3^{2-}, *in situ* CO_2(g), and CO_2(aq) vary in the spacing where the local pH changes, and the distance of spacing is the most significant descriptor for the concentration of reactant, *in situ* CO_2(g).

In a prior study,[5] at a CEL:catalyst spacing of ~60 μm (Figures 1F, 1G, and S7), the volume fraction of CO_2(g) ([CO_2(g)]) at the plane of the catalyst was found to be

[1]Department of Electrical and Computer Engineering, University of Toronto, 35 St George Street, Toronto, ON M5S 1A4, Canada

[2]Clean Energy Research Center, Korea Institute of Science and Technology (KIST), Seoul 02792, Republic of Korea

[3]Department of Mechanical and Industrial Engineering, University of Toronto, 5 King's College Road, Toronto, ON M5S 3G8, Canada

[4]Department of Chemistry, Northwestern University, Evanston, IL 60208, USA

[5]Department of Electrical and Computer Engineering, Northwestern University, Evanston, IL 60208, USA

[6]These authors contributed equally

[7]Lead contact

*Correspondence: ted.sargent@northwestern.edu

https://doi.org/10.1016/j.joule.2023.05.003

Table 1. Energy analysis of different systems: alkaline CO_2RR, neutral CO_2RR, acidic CO_2RR, and carbonate electrolysis

System	Alkaline CO_2RR	Neutral CO_2RR	Acidic CO_2RR	Carbonate electrolysis
Full cell voltage (V)	2.4	3.9	3.4	4.1
C_2H_4 selectivity (%)	70	66	24	34
Current density (mA cm^{-2})	150	315	200	300
Energy efficiency (%)	34	19	8	10
CO_2 utilization (%)	5	11	76	100[a]
C_2H_4 concentration at the outlet (wt %)	4	8	19	56
CO_2 concentration at the outlet (wt %)	93	88	56	0
Energy cost (GJ/tonne of C_2H_4)				
Upstream generation	28	28	28	3
Electrolysis	142	244	586	499
Product separation	115	55	18	2
Anode separation	0	57	0	0
Carbonate generation	198	0	0	0
Total	483	384	631	504

[a]No detectable CO_2 gas in the cathodic/anodic tail gas.

~2 vol % with balanced gases of H_2 and C_2H_4 at current densities of 200–350 mA cm^{-2} (Figure 1C)—yet [CO_2(g)] is required to rise above 4 vol % at the catalyst to reach a meaningful conversion rate of C_{2+} partial current densities of 100+ mA cm^{-2} (Notes S3 and S4; Figure S8).

We studied these effects further, noting that if the CEL and the catalyst are closely spaced (Figures 1D and 1E), the local pH at the CEL goes only as low as pH 10, and CO_3^{2-} and OH^- diffusion neutralize the acidic CEL surface,[29,30] leading to no *in situ* CO_2(g) generation at applied current densities of 200–350 mA cm^{-2} (Figure S9). By contrast, when we varied the CEL:catalyst spacing over the range 100–300 μm (Figures 1H–1K), we noted the opportunity to achieve the desired conditions of low pH (<4) at the CEL for *in situ* CO_2(g) generation and [CO_2(g)] > 4 vol % at the catalyst layer (CL) to trigger CO_2RR toward C_{2+} production. At the CL, the pH is above 13 since hydroxide ions are produced from CO_2RR. This high local pH accelerated the C–C coupling needed for C_{2+} to dominate over C_1.[31,32] The pH gradient was measured using pH-sensitive dyes (Note S5). We observed a progressive pH increase from pH ~2 at the CEL surface to ~12 at the edge of the interposer in the system designed for the experimental study of pH.

For the spacing range of 130–270 μm, optimal conditions, including [CO_2(g)] > 4 vol % and the desired local pH, were achieved at the current density range 250–350 mA cm^{-2}, a regime of applied interest.[33,34] In the case wherein the amount of carbonate is limited due to a small spacing, such as <130 μm, there is no increase in the *in situ* CO_2(g) concentration at higher current densities (Figure S3). However, the current density influences the rate of proton diffusion through the CEL: more protons diffuse at higher current densities and *in situ* CO_2(g) generally increases (Figure 1C). Increasing the spacing to >130 μm promotes carbonate-rich conditions, which provide more opportunities for protons to react with carbonate (Figures S4 and S5). However, [CO_2(g)] decreases at a spacing >540 μm due to an increased possibility of *in situ* CO_2 capture over long distances in the layer (Figure S6).

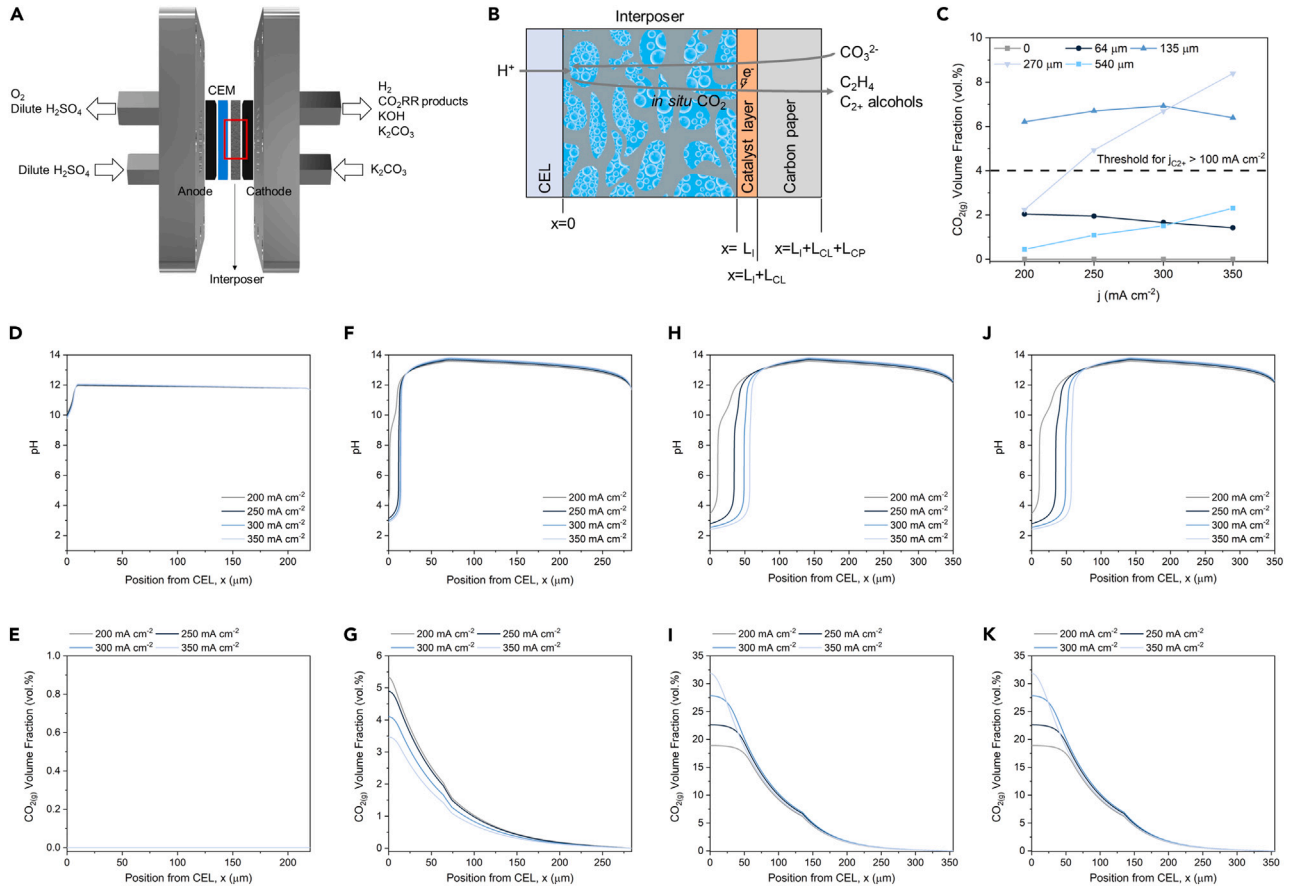

Figure 1. Carbonate electrolysis system employing an interposer

(A) System diagram of CO_3^{2-}-fed electrolyzer. The cathode and anode are separated by the cation-exchange membrane (CEM) and the mixed cellulose ester (MCE) membrane as the interposer. K_2CO_3 is fed to the electrolyzer, and *in situ* CO_2 is converted into CO_2-derived products. KOH is generated at the cathode from *in situ* CO_2 reduction reaction (CO_2RR). 0.5 M H_2SO_4 is fed at the anode, and the anodic oxygen evolution reaction supplies protons.

(B) Schematic of cation-exchange layer (CEL), the interposer, catalyst layer (CL), and carbon paper (CP). The MCE membrane has a pore where the carbonate liquid-phase and gas-phase *in situ* CO_2 are distributed.

(C) CO_2(g) volume fraction for different spacing (L_I) conditions, 0, 64, 135, and 540 μm at current densities of 200, 250, 300, and 350 mA cm^{-2} in 1.5 M of K_2CO_3 electrolyte.

(D, F, H, and J) pH profile of 0, 64, 135, and 540 μm spacing, respectively, at the applied current densities from 200 to 350 mA cm^{-2} in 1.5 M of K_2CO_3 electrolyte.

(E, G, I, and K) *In situ* CO_2(g) volume fraction profile of 0, 64, 135, and 540 μm spacing, respectively, at the applied current densities from 200 to 350 mA cm^{-2} in 1.5 M K_2CO_3 electrolyte.

Carbonate electrolysis system employing an interposer

We then turned to the experimental implementation of these concepts (Figure 1A). We needed an approach to construct a well-defined spacing—in effect, a stand-off—between the CEL and electrocatalyst. We used a hydrophilic membrane as an interposer and explored different interposer material compositions (Note S6; Figures S10–S12). We observed that C_{2+} FE was improved in a higher porosity system. We account for these observations via faster diffusion of species which enabled a higher concentration of CO_2(g) at the CL.

In light of these findings, we focused on a hydrophilic mixed cellulose ester (MCE) interposer, a highly porous medium (material porosity > 84%) with a selection of thicknesses ranging from 130 to 540 μm (Figure S13). We then moved to a cation-exchange membrane (CEM) in the system to transport protons from the anodic oxygen

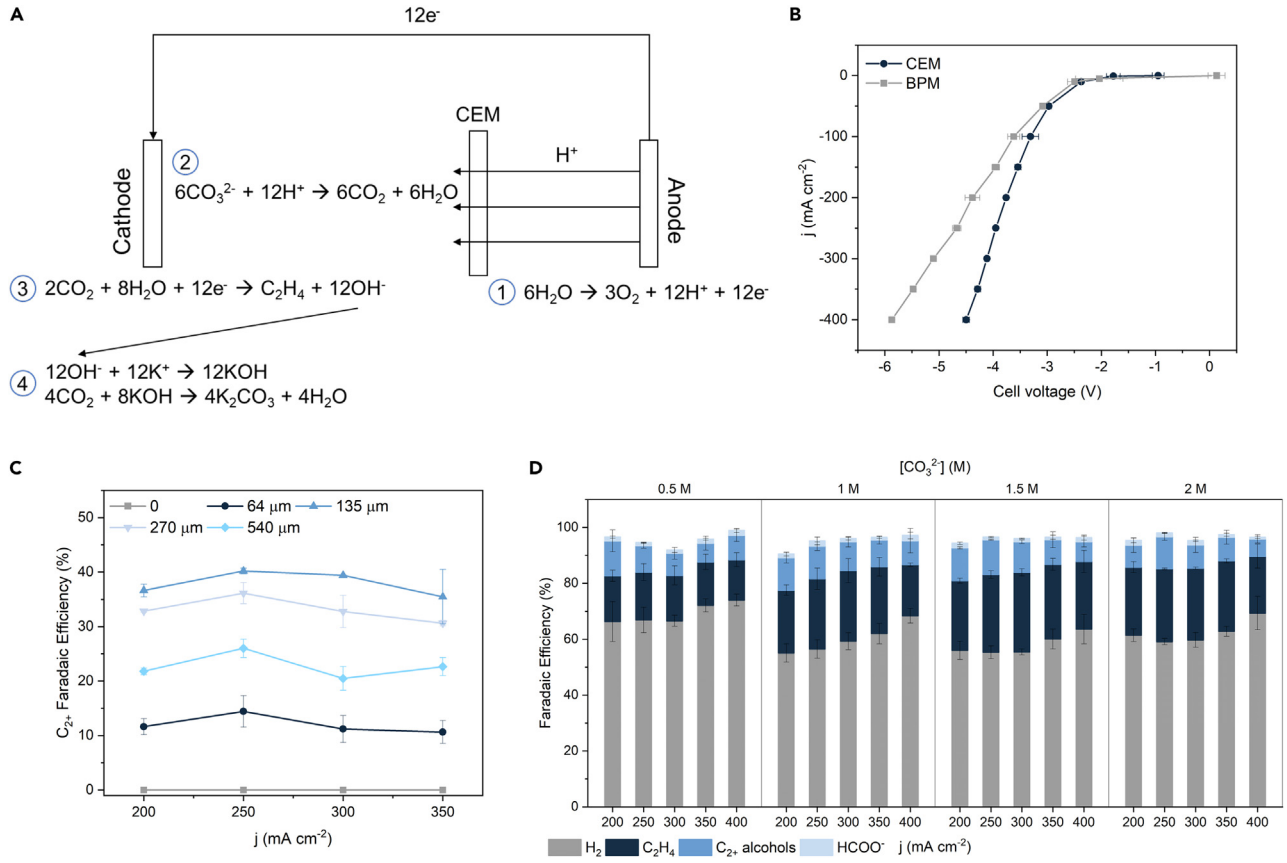

Figure 2. Carbonate electrolysis

(A) Chemical reactions of carbonate electrolysis with the cation-exchange membrane (CEM). OER at the anodic side supplies protons to the cathodic side. Carbonate is converted into *in situ* CO_2 via the carbonate/proton reactions. CO_2 reduction reaction (CO_2RR) occurs with a Cu electrocatalyst. CO_2-derived products are generated, and OH^- is produced during *in situ* CO_2RR. Unreacted CO_2 is captured by OH^-.

(B) Full cell J-V curve with Cu electrocatalyst with a CEM and a bipolar membrane (BPM) in 1.5 M of K_2CO_3 electrolyte with 135 μm interposer. Higher voltage is observed in the case of the BPM system compared with the CEM system due to water dissociation overpotential. All experiments were repeated three times to enable reporting of the average and standard error.

(C) C_{2+} Faradaic efficiency (FE) of carbonate electrolysis with Cu electrocatalyst in 1.5 M of K_2CO_3 electrolyte with the different thickness of interposer from 0 to 540 μm. All experiments were repeated three times to enable reporting of the average and standard error.

(D) Product distribution for different concentrations of K_2CO_3 electrolyte from 0.5 to 2 M with a 135 μm interposer. C_{2+} alcohols Faradaic efficiency includes C_2H_5OH and C_3H_7OH. All experiments were repeated three times to enable reporting of the average and standard error.

evolution reaction (OER) (Figure 2A)—an improvement that enabled reduced full cell potential compared with a BPM system (Figure 2B). The CEM system may supply more protons to the cathodic side than the BPM system due to the concentration gradient, neutralizing the capture species (OH^-). However, we observed a similar product distribution for both the BPM system and CEM system (Figure S14), indicating that excess proton diffusion in the CEM system is negligible when using 0.5 M H_2SO_4 as an anolyte (Note S7).

Experimentally, we first reconfirmed the findings of prior studies that, at ~60 μm spacing, FE to C_{2+} resides below 14% at 250 mA cm^{-2}. When we optimized interposer thickness of 130–270 μm, we achieved a much-increased C_{2+} FE of 40% at 250 mA cm^{-2} (Figure 2C). When the distance is smaller than 135 μm or larger than 540 μm, a lower rate of C_{2+} product generation is seen, the result of the limited concentration of *in situ* CO_2(g) (Figure 1C). In all cases, the only C_1 product detected was $HCOO^-$ with FE below 2%. No CO, CH_4, and CO_2 were detected for all applied

current densities and different concentrations of carbonate electrolyte in the interposer system (Figures 2D and S11). The product distribution, including high C_{2+} FE and negligible CO FE, was also observed in a simulated carbonate electrolysis system with CO_2-depleted conditions (Note S3). The experimental studies suggest that in the carbonate electrolysis system, low [CO_2(g)] and slow *in situ* CO_2 flux contribute to steering C–C coupling by achieving locally concentrated CO and the enhanced residence time of CO. In the outlet stream, gaseous C_1 products and CO_2 were <0.9 wt % (0.1 vol %) based on the detection limit of the gas chromatography (GC): CO for 24 ppm, CH_4 for 56 ppm, and CO_2 for 1,000 ppm, respectively (experimental procedures). To investigate whether carbonate was the source of carbon in electroreduction, we used ^{13}C labeled CO_3^{2-}, and the isotope experiment result ruled out any chemical reactions of interposer, cathode, and dissolved CO_2 (Figure S15). To test for the possibility of chemical reactions related to the MCE membrane or its possible decomposition products, we compared electrochemical performance in two conditions: (1) carbonate electrolyte and (2) carbonate electrolyte with a dispersed MCE membrane in a PVDF interposer system (Figure S16). In both cases, we observed a C_{2+} FE of ~15% at the applied current density of 200 and 300 mA cm^{-2}. We also conducted nuclear magnetic resonance (NMR) analysis to examine the chemical decomposition of the MCE membrane after long-term electrolysis of carbonate. We only detected signals for CO_2-derived products, which supports that there is no chemical decomposition or reactions of MCE in the carbonate electrolysis system (Figure S17).

Improved catalyst for carbonate electrolysis

We turned to further system tuning toward increased C_{2+} FE. We posited that a portion of *in situ* CO_2 is converted into CO_3^{2-} at the catalyst surface due to the highly alkaline conditions.[31] We, therefore, sought catalyst-design strategies to convert CO_2 to CO with faster kinetics at the catalyst surface to preserve the reactant. We used molecularly dispersed cobalt phthalocyanines on carbon nanotubes (CoPCs-CNTs) known to produce CO from CO_2 with high turnover frequencies (Figure 3A).[35,36] We fabricated the layer-by-layer catalyst via airbrushing. The CoPC-CNTs layer is uniformly distributed on the Cu layer as shown in the scanning electron microscopy (SEM) image (Figure 3B). X-ray photoelectron spectroscopy (XPS) and energy-dispersive X-ray spectroscopy (EDS) confirm the existence of cobalt at the surface (Figures S18 and S19).

The product distribution now showed a considerable further improvement: the C_{2+} total FE now rose to 47% at 300 mA cm^{-2} (Figure 3C). The C_2H_4 FE is 34%, resulting in 56 wt % of C_2H_4 in the product gas stream due to the absence of gaseous C_1 products and unreacted CO_2. The C_{2+} alcohols FE is 13% including 12% C_2H_5OH FE and 1% C_3H_7OH FE. As shown in Figure 3D, we achieve 140+ mA cm^{-2} of C_{2+} partial current density at −4.1 V.

Continuous operation of capture-and-electrolysis system

We then constructed a prototype that operates both CO_2 capture and electrolysis on a continuous basis (Figures 4A and S20). The KOH capture liquid is regenerated during carbonate electrolysis as shown in the chemical balance (Figure 2A; Note S7). We recycled the resultant KOH solution to continuously capture additional CO_2, converting it into K_2CO_3. There are two reservoirs: the absorber is for CO_2 capture and the electrolyte reservoir provides the carbonate to the liquid-fed electrolyzer. Two reservoirs and the electrolyzer are connected by peripheral pumps circulating the capture liquid. During the electrolysis of carbonate into C_2H_4 and C_{2+} alcohols, generated OH^- returns to the absorber. We demonstrated capture-and-electrolysis

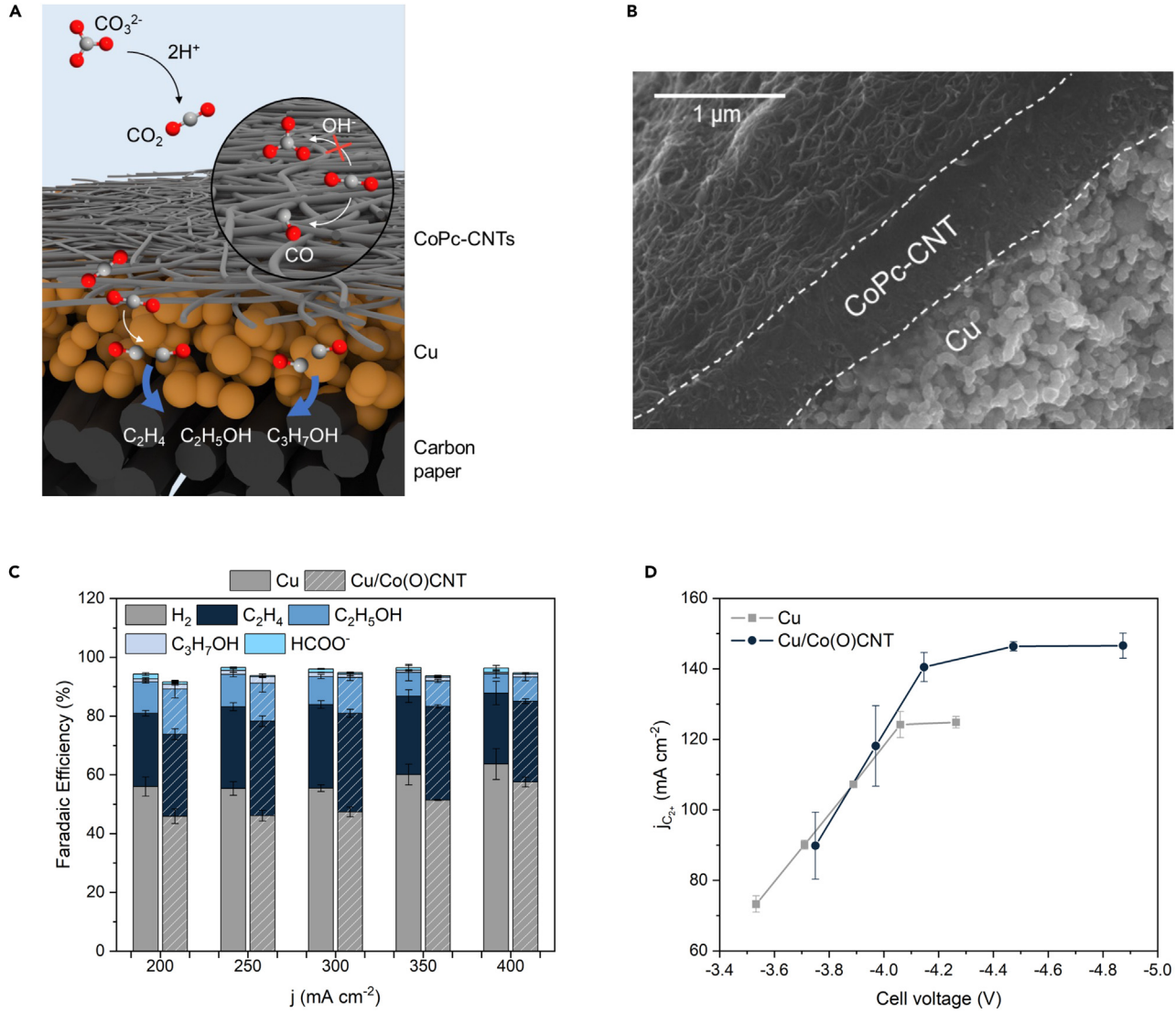

Figure 3. Electrochemical performance of improved catalyst for carbonate electrolysis

(A) Illustration of the improved catalyst depositing CoPc-CNTs layer onto Cu electrocatalyst.

(B) Scanning electron microscope image of Cu/CoPc-CNTs layer.

(C) Product distribution of control Cu electrocatalyst and Cu/CoPC-CNTs catalyst at applied current densities from 200 to 400 mA cm^{-2}. 1.5 M K_2CO_3 and 135 μm MCE membranes are used as the electrolyte and interposer, respectively. All experiments were repeated three times to enable reporting of the average and standard error.

(D) C_{2+} partial current density vs. full cell voltage for Cu electrocatalyst and Cu/CoPc-CNTs electrocatalyst. All experiments were repeated three times to enable reporting of the average and standard error.

sustained over 20 h (Figure 4B) at the current density of 200 mA cm^{-2}, with the C_{2+} FE consistently in the range of 36%–42%. The pH of reservoirs remains 11.8 for the absorber, 11.9 for the electrolyte, and 1.8 for the anolyte (Table S7). We found that after 10 h of operation, performance does show a decline (Figure 4B). We studied the cause, finding that the pore structure of the MCE membrane degrades in alkali solution, producing an increase of full cell voltage and hydrogen evolution recations (HER). It will be important to seek interposer materials that are stable under relevant conditions.

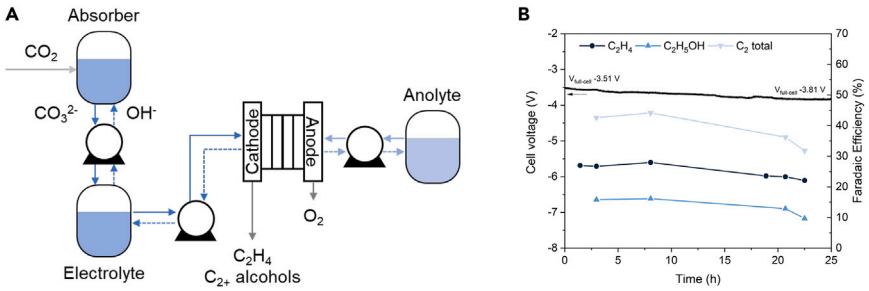

Figure 4. Extended operation with CO_2 capture liquid stream

(A) The schematic illustrates the process flow of the capture-and-electrolysis system. CO_2 is captured with 3 M KOH at the absorber until the pH of the solution reaches to ~12, and the capture liquid, K_2CO_3, is fed to the electrolyzer. The lean capture liquid, KOH, returns to the absorber.

(B) Long-term operation for the capture-and-electrolysis system. The experiment was performed with a Cu/CoPc-CNTs electrocatalyst and 135 μm interposer. Cell voltage and Faradaic efficiency of C_2H_4, C_2H_5OH, and C_{2+} products are noted during the operation.

Economic assessments of carbonate electrolysis

In Table 1, we offer an analysis that also estimates energy costs—associated with upstream generation for the gas-phase CO_2 and carbonate capture solutions, electrolysis, separation, and carbonate regeneration—in systems including alkaline CO_2 electrolysis,[31] neutral CO_2 electrolysis in a membrane electrode assembly (MEA),[37] and acidic CO_2 electrolysis[23] vs. this present work (details in Note S8). Both the gaseous CO_2 approaches in alkaline and neutral conditions experience a CO_2 utilization limit (≤25%) since CO_2 gas is lost to carbonate formation, and carbonate crosses over to the anodic side during electrolysis.[19,38] The product gas stream is diluted by unreacted CO_2 for all gas-phase CO_2 approaches. In comparison, the carbonate electrolysis system generates a product stream that does not contain CO_2.

As is now well-established, alkaline electrolysis leads to a high rate of CO_2 loss—typically 95% is lost to carbonate and unreacted form—leading to an estimated 310 GJ/tonne of C_2H_4 for regeneration/separation energy costs. This cost is equal to 7× the lower heating value (LHV) of C_2H_4.

Neutral CO_2RR still produces a high CO_2 stream in the cathodic outlet and this necessitates ~60 GJ/tonne of C_2H_4 investment in CO_2 separation from the cathode. Furthermore, CO_2 crossover mandates a separation of the O_2-containing stream in the anodic outlet contributing to ~60 GJ/tonne of C_2H_4 of separation energy cost. The total separation cost is equal to 2× the LHV of C_2H_4.

The acidic CO_2RR system enables an estimated decrease in product separation cost to ~18 GJ/tonne of C_2H_4 with a high CO_2 utilization efficiency of ~76%. Unlike alkaline and neutral CO_2RR, no CO_2 is lost as carbonate formation and crossover, eliminating the need for processes to regenerate the carbonate or crossover CO_2. However, there is a trade-off between FE and CO_2 utilization in presently available acidic CO_2RR systems,[21,23] with these systems still requiring energy-intensive DAC to generate gaseous CO_2 costing roughly ~28 GJ/tonne of C_2H_4.

In contrast, the carbonate electrolysis to the C_2H_4 system produces a CO_2 concentration that is undetectable in the cathode stream. This obviates the energy needed to separate CO_2 and C_2H_4. What remains is 2 GJ/tonne of C_2H_4 to remove H_2 and H_2O from the cathodic outlet stream. The low separation cost originates from the high concentration of C_2H_4 and the absence of CO_2. Furthermore, the system lowers the upstream generation cost by a factor of ~10 by bypassing the thermal swing of DAC.

We note the need to improve further the energy efficiency of the reactive capture electrolyzer itself. We offer that further studies of *in situ* CO_2 diffusion in the interposer, and further advances in interposer/electrocatalyst design, may contribute toward this goal.

DISCUSSION

Interposer and catalyst joint design enabled us herein to electroproduce 56 wt % C_2H_4 from a carbonate solution with no detected CO_2 in the gas stream. To achieve this result, we focused on local pH and reactant concentration as metrics driving the performance of an electrochemical reactive capture system. The carbonate electrolysis system produces a gas stream that is undiluted by CO_2 and accomplishes complete CO_2 utilization, reducing regeneration/separation costs.

EXPERIMENTAL PROCEDURES

Resource availability

Lead contact

Further information and requests for resources should be directed to and will be fulfilled by the lead contact, Edward Sargent (ted.sargent@utoronto.ca).

Materials availability

This study did not generate new unique reagents.

Data and code availability

The data presented in this work are available from the corresponding authors upon reasonable request.

Catalyst preparation

All reagents used in this work were purchased from suppliers without further purification. Cu catalysts (US Research Nanomaterials) were prepared by spray-coating Cu nanoparticle ink onto carbon paper (Freudenberg H23, Fuel Cell Store). Cu nanoparticles (80 mg) were dispersed in a mixture of 12 mL methanol and 160 μL Nafion solution and then sonicated for 3 h. The Cu nanoparticle ink was spray-coated on the carbon paper with a loading of ~4 mg/cm^2 and dried under atmospheric conditions. The Cu catalysts were used for electrochemical characterization for carbonate electrolysis in a MEA cell.

For simulated carbonate electrolysis experiments in a flow cell, Cu catalysts were prepared by spray-coating Cu nanoparticles onto a polytetrafluoroethylene(PTFE) substrate (450 nm pore size). Cu nanoparticles (80 mg) were dispersed in a mixture of 12 mL methanol and 160 μL Nafion solution and then sonicated for 3 h. The Cu nanoparticle ink was spray-coated on the PTFE substrate with a loading of ~4 mg/cm^2 and dried under atmospheric conditions.

Cobalt phthalocyanines (CoPc), carboxylic acid-functionalized carbon nanotubes (CNTs), and dimethylformamide (DMF) were purchased from Sigma Aldrich and used without further treatment. CoPc-CNTs catalyst was synthesized with modification from the previous report.[35] 30 mg of carboxylic acid-functionalized CNTs were dispersed in DMF (20 mL, solution 1) and sonicated for 1 h. A calculated amount of CoPc was dispersed in DMF (20 mL, solution 2) and sonicated for 1 h. Solutions 1 and 2 were mixed and sonicated for 30 min. After sonication, the mixture solution was stirred for 24 h at room temperature. CoPc-CNTs were centrifuged and washed with DMF, ethanol, and H_2O, followed by freeze drying to obtain the final catalyst material.

CoPc-CNTs/Cu catalysts were prepared by spray-coating on the prepared Cu/carbon paper. CoPc-CNTs were dispersed in a mixture of 3 mL ethanol and 50 μL Nafion solution and then sonicated for 1 h. The CoPc-CNTs nanoparticle ink was spray-coated on the Cu/carbon paper with a loading of ~0.3 mg/cm^2 and dried under atmospheric conditions.

Electrochemical performance

Electrochemical data were collected using an electrochemical station (PGSTAT204) in an MEA system and a flow cell system. All experiments were repeated three times to enable reporting of the average and standard error. Electrolysis was maintained for at least 30 min prior to collecting gas and liquid samples. For the MEA system with carbonate electrolysis, the as-prepared Cu/carbon paper catalyst was used as the cathode in varying the distances between the cathode and a CEM: 0, 135, 270, and 540 μm with MCE membrane and varying catholyte: 0.5, 1, 1.5, and 2 M of K_2CO_3. The anolyte was a 0.5 M H_2SO_4 solution. Titanium foam-supported iridium oxide (IrO_x/Ti) was used as the anode OER catalyst. Nafion 117 membrane was used to separate the two electrodes. The catholyte and anolyte were circulated using a peristaltic pump.

For the simulated carbonate electrolysis in a flow cell, the as-prepared Cu/PTFE catalyst was used as the working electrode in the catholyte (1.5 M of K_2CO_3) in varying gas-phase CO_2 partial pressure in the N_2 stream, maintaining the total flow rate of 50 sccm and gas-phase CO_2 flow rate. The anolyte was always a 1 M KOH solution. Ni foam and 3 M Ag/AgCl were used as the anode and reference electrodes, respectively. An anion exchange membrane (Fumasep FAA-3-PK-130) was used to separate the cathode and the anode. The catholyte and anolyte were circulated using a peristaltic pump.

The gas-phase products were analyzed using GC (Shimadzu 2014, PerkinElmer Clarus 580) equipped with a thermal conductivity detector (TCD) and a flame ionization detector (FID). All measurements were repeated three times to report the average and standard error. The liquid phase products were analyzed with a 600 MHz Agilent DD2 ^{1}H NMR.

The detection limit of GC for gas-phase products (CO and CH_4) is measured by varying the concentration of gas in the CO_2 stream. The ppm level of the gas-phase product is injected three times. The area of a peak is linearly correlated to the concentration when the area value is plotted at the y axis, and the concentration is at the x axis. The intercept of the x axis represents the detection limits of gas concentration. The detection limit of CO_2 is measured by injecting a different air volume from 1 to 5 mL. The CO_2 concentration in the air is assumed at 400 ppm.

Material characterization

The Cu/CoPc-CNTs catalyst morphology was characterized by field emission SEM (Hitachi, SU5000). The surface composition was analyzed with ThermoFisher Scientific K-alpha XPS using Al Kα X-ray radiation. XPS spectra were calibrated with the C 1s peak at 284.5 eV. SEM-EDS was conducted by JEOL JSM-7900FLV SEM at an accelerating voltage of 10 kV with backscattered electron detection, which is equipped with a light-element X-ray detector and an Oxford Aztec energy-dispersive X-ray analysis system.

Fluorescence measurements

For the simulated interposer system in a H-cell, a carbon paper, Pt mesh, and Ag/AgCl reference electrode were used as the working, counter, and reference electrodes, respectively. 0.2 M K_2CO_3 and 0.5 M H_2SO_4 electrolytes were used as a catholyte and an anolyte, respectively. Nafion 117 membrane was used to separate the cathode

part and the anode part. Molecular Probes LysoSensor Green DND 189 (LSG) was used to measure a pH range of 1–6, and 5(6)-carboxynaphthofluorescein (CNF) was used to measure neutral and alkaline pH from 6 to 14. Using 365 nm of UV light, the fluorescence emissions were collected with a spectrometer (Ocean Optics, QE Pro).

Stability test

Two reservoirs were connected by peristaltic pumps (Figure S17). CO_2 is purged into the absorber with 3 M KOH until the pH of the solution reaches to ~12, and an electrolyte reservoir provides the carbonate solution to the electrolyzer. The carbonate electrolyte is pumped to the MEA cell with no gas purging. The regenerated KOH solution returns to the absorber, where it captures CO_2 in the form of CO_3^{2-}. The gas products from the electrolyte reservoir were monitored with GC injection.

SUPPLEMENTAL INFORMATION

Supplemental information can be found online at https://doi.org/10.1016/j.joule.2023.05.003.

ACKNOWLEDGMENTS

This work was financially supported by the Ontario Research Foundation: Research Excellence Program, the Natural Sciences and Engineering Research Council (NSERC) of Canada. H.L. and E.S. acknowledge the financial support from Northwestern University's start-up grant.

AUTHOR CONTRIBUTIONS

E.S. supervised the work. G.L. contributed to the main idea and designed experiments. A.S.R. contributed to multiphysic modeling. B.-H.L. fabricated the electrocatalyst and contributed to material characterization. J.Z., D.H.W., and Y.C.X. contributed to the electrochemical experiments. J.P.E. and Y.Z. performed the energy analysis. M.G.L. conducted C13 labeling experiments. E.D.J. conducted local pH measurements. J.A., S.P., and H.L. conducted material characterization. F.A. performed voltage breakdown analysis. T.A. and S.L. assisted in the multiphysic modeling. I.G., R.K.M, R.D., C.P.O., Z.C., and D.S. contributed to data analysis and manuscript preparation.

DECLARATION OF INTERESTS

The authors declare no competing interests.

Received: January 20, 2023
Revised: May 3, 2023
Accepted: May 4, 2023
Published: May 26, 2023

REFERENCES

1. Brethomé, F.M., Williams, N.J., Seipp, C.A., Kidder, M.K., and Custelcean, R. (2018). Direct air capture of CO2 via aqueous-phase absorption and crystalline-phase release using concentrated solar power. Nat. Energy *3*, 553–559. https://doi.org/10.1038/s41560-018-0150-z.

2. Kätelhön, A., Meys, R., Deutz, S., Suh, S., and Bardow, A. (2019). Climate change mitigation potential of carbon capture and utilization in the chemical industry. Proc. Natl. Acad. Sci. USA *116*, 11187–11194. https://doi.org/10.1073/pnas.1821029116.

3. Socolow, R., Desmond, M., Aines, R., Blackstock, J., Bolland, O., Kaarsberg, T., Lewis, N., Mazzotti, M., Pfeffer, A., and Sawyer, K. (2011). Direct air capture of CO_2 with chemicals: a technology assessment for the APS panel on public affairs (American Physical Society). http://www.aps.org/policy/reports/assessments/upload/dac2011.pdf.

4. Lee, G., Li, Y.C., Kim, J.-Y., Peng, T., Nam, D.-H., Sedighian Rasouli, A., Li, F., Luo, M., Ip, A.H., Joo, Y.-C., et al. (2021). Electrochemical upgrade of CO_2 from amine capture solution. Nat. Energy *6*, 46–53. https://doi.org/10.1038/s41560-020-00735-z.

5. Li, Y.C., Lee, G., Yuan, T., Wang, Y., Nam, D.-H., Wang, Z., García de Arquer, F.P., Lum, Y., Dinh, C.-T., Voznyy, O., et al. (2019). CO_2 electroreduction from carbonate electrolyte. ACS Energy Lett. *4*,

1427–1431. https://doi.org/10.1021/acsenergylett.9b00975.

6. Li, T., Lees, E.W., Goldman, M., Salvatore, D.A., Weekes, D.M., and Berlinguette, C.P. (2019). Electrolytic conversion of bicarbonate into CO in a flow cell. Joule *3*, 1487–1497. https://doi.org/10.1016/j.joule.2019.05.021.

7. Zhang, Z., Lees, E.W., Habibzadeh, F., Salvatore, D.A., Ren, S., Simpson, G.L., Wheeler, D.G., Liu, A., and Berlinguette, C.P. (2022). Porous metal electrodes enable efficient electrolysis of carbon capture solutions. Energy Environ. Sci. *15*, 705–713. https://doi.org/10.1039/D1EE02608A.

8. Xiao, Y.C., Gabardo, C.M., Liu, S., Lee, G., Zhao, Y., O'Brien, C.P., Miao, R.K., Xu, Y., Edwards, J.P., and Fan, M. (2023). Direct carbonate electrolysis into pure syngas. EES Catal. *1*, 54–61.

9. Kar, S., Goeppert, A., and Prakash, G.K.S. (2019). Integrated CO_2 capture and conversion to formate and methanol: connecting two threads. Acc. Chem. Res. *52*, 2892–2903. https://doi.org/10.1021/acs.accounts.9b00324.

10. Kothandaraman, J., Saavedra Lopez, J., Jiang, Y., Walter, E.D., Burton, S.D., Dagle, R.A., and Heldebrant, D.J. (2021). Integrated capture and conversion of CO_2 to methane using a water-lean, post-combustion CO_2 capture solvent. ChemSusChem *14*, 4812–4819. https://doi.org/10.1002/cssc.202101590.

11. Sen, R., Goeppert, A., Kar, S., and Prakash, G.K.S. (2020). Hydroxide based integrated CO_2 capture from air and conversion to methanol. J. Am. Chem. Soc. *142*, 4544–4549. https://doi.org/10.1021/jacs.9b12711.

12. GlobeNewswire. PrecedenceResearch (2021). Ethanol market size worth around USD 155.6 billion by 2030. t. https://www.globenewswire.com/news-release/2021/01/18/2160198/0/en/Ethanol-Market-Size-Worth-Around-USD-155-6-Billion-by-2030.html#:~:text=The%20global%20ethanol%20market%20size,5.2%25%20from%202021%20to%202030.

13. Polaris Market Research (2021). Ethylene market size worth $230.7 billion by 2029|CAGR: 5.5%. https://www.polarismarketresearch.com/press-releases/ethylene-market.

14. Polaris Market Research (2017). Feed acidifiers market size worth $2.03 billion by 2026|CAGR: 4.5%. https://www.polarismarketresearch.com/press-releases/feed-acidifiers-market.

15. Polaris Market Research (2021). Carbon dioxide market size worth $9.91 billion by 2029|CAGR: 4.1%. https://www.polarismarketresearch.com/press-releases/carbon-dioxide-co2-market.

16. Keith, D.W., Holmes, G., St. Angelo, D., and Heidel, K. (2018). A process for capturing CO2 from the atmosphere. Joule *2*, 1573–1594. https://doi.org/10.1016/j.joule.2018.05.006.

17. García de Arquer, F.P.G.d., Dinh, C.T., Ozden, A., Wicks, J., McCallum, C., Kirmani, A.R., Nam, D.H., Gabardo, C., Seifitokaldani, A., Wang, X., et al. (2020). CO_2 electrolysis to multicarbon products at activities greater than 1 A cm^{-2}. Science *367*, 661–666. https://doi.org/10.1126/science.aay4217.

18. Li, F., Thevenon, A., Rosas-Hernández, A., Wang, Z., Li, Y., Gabardo, C.M., Ozden, A., Dinh, C.T., Li, J., Wang, Y., et al. (2020). Molecular tuning of CO_2-to-ethylene conversion. Nature *577*, 509–513. https://doi.org/10.1038/s41586-019-1782-2.

19. Rabinowitz, J.A., and Kanan, M.W. (2020). The future of low-temperature carbon dioxide electrolysis depends on solving one basic problem. Nat. Commun. *11*, 5231.

20. Alerte, T., Edwards, J.P., Gabardo, C.M., O'Brien, C.P., Gaona, A., Wicks, J., Obradović, A., Sarkar, A., Jaffer, S.A., MacLean, H.L., et al. (2021). Downstream of the CO2 electrolyzer: assessing the energy intensity of product separation. ACS Energy Lett. *6*, 4405–4412. https://doi.org/10.1021/acsenergylett.1c02263.

21. Huang, J.E., Li, F., Ozden, A., Sedighian Rasouli, A., García de Arquer, F.P., Liu, S., Zhang, S., Luo, M., Wang, X., Lum, Y., et al. (2021). CO_2 electrolysis to multicarbon products in strong acid. Science *372*, 1074–1078. https://doi.org/10.1126/science.abg6582.

22. O'Brien, C.P., Miao, R.K., Liu, S., Xu, Y., Lee, G., Robb, A., Huang, J.E., Xie, K., Bertens, K., Gabardo, C.M., et al. (2021). Single pass CO_2 conversion exceeding 85% in the electrosynthesis of multicarbon products via local CO_2 regeneration. ACS Energy Lett. *6*, 2952–2959. https://doi.org/10.1021/acsenergylett.1c01122.

23. Zhao, Y., Hao, L., Ozden, A., Liu, S., Miao, R.K., Ou, P., Alkayyali, T., Zhang, S., Ning, J., Liang, Y., et al. (2023). Conversion of CO_2 to multicarbon products in strong acid by controlling the catalyst microenvironment. Nat. Synth. https://doi.org/10.1038/s44160-022-00234-x.

24. Gabardo, C.M., O'Brien, C.P., Edwards, J.P., McCallum, C., Xu, Y., Dinh, C.-T., Li, J., Sargent, E.H., and Sinton, D. (2019). Continuous carbon dioxide electroreduction to concentrated multi-carbon products using a membrane electrode assembly. Joule *3*, 2777–2791. https://doi.org/10.1016/j.joule.2019.07.021.

25. Kim, C., Bui, J.C., Luo, X., Cooper, J.K., Kusoglu, A., Weber, A.Z., and Bell, A.T. (2021). Tailored catalyst microenvironments for CO_2 electroreduction to multicarbon products on copper using bilayer ionomer coatings. Nat. Energy *6*, 1026–1034. https://doi.org/10.1038/s41560-021-00920-8.

26. Idem, R., Supap, T., Shi, H., Gelowitz, D., Ball, M., Campbell, C., and Tontiwachwuthikul, P. (2015). Practical experience in post-combustion CO_2 capture using reactive solvents in large pilot and demonstration plants. Int. J. Greenhouse Gas Control *40*, 6–25. https://doi.org/10.1016/j.ijggc.2015.06.005.

27. Lin, Y.-J., and Rochelle, G.T. (2016). Approaching a reversible stripping process for CO_2 capture. Chem. Eng. J. *283*, 1033–1043. https://doi.org/10.1016/j.cej.2015.08.086.

28. Greenblatt, J.B., Miller, D.J., Ager, J.W., Houle, F.A., and Sharp, I.D. (2018). The technical and energetic challenges of separating (photo) electrochemical carbon dioxide reduction products. Joule *2*, 381–420. https://doi.org/10.1016/j.joule.2018.01.014.

29. Lees, E.W., Bui, J.C., Song, D., Weber, A.Z., and Berlinguette, C.P. (2022). Continuum model to define the chemistry and mass transfer in a bicarbonate electrolyzer. ACS Energy Lett. *7*, 834–842. https://doi.org/10.1021/acsenergylett.1c02522.

30. Kas, R., Yang, K., Yewale, G.P., Crow, A., Burdyny, T., and Smith, W.A. (2022). Modeling the local environment within porous electrode during electrochemical reduction of bicarbonate. Ind. Eng. Chem. Res. *61*, 10461–10473. https://doi.org/10.1021/acs.iecr.2c00352.

31. Dinh, C.T., Burdyny, T., Kibria, M.G., Seifitokaldani, A., Gabardo, C.M., García de Arquer, F.P., Kiani, A., Edwards, J.P., De Luna, P., Bushuyev, O.S., et al. (2018). CO_2 electroreduction to ethylene via hydroxide-mediated copper catalysis at an abrupt interface. Science *360*, 783–787. https://doi.org/10.1126/science.aas9100.

32. Varela, A.S., Kroschel, M., Reier, T., and Strasser, P. (2016). Controlling the selectivity of CO_2 electroreduction on copper: the effect of the electrolyte concentration and the importance of the local pH. Cat. Today *260*, 8–13. https://doi.org/10.1016/j.cattod.2015.06.009.

33. Jouny, M., Luc, W., and Jiao, F. (2018). General techno-economic analysis of CO_2 electrolysis systems. Ind. Eng. Chem. Res. *57*, 2165–2177. https://doi.org/10.1021/acs.iecr.7b03514.

34. Shin, H., Hansen, K.U., and Jiao, F. (2021). Techno-economic assessment of low-temperature carbon dioxide electrolysis. Nat. Sustain. *4*, 911–919. https://doi.org/10.1038/s41893-021-00739-x.

35. Zhang, X., Wang, Y., Gu, M., Wang, M., Zhang, Z., Pan, W., Jiang, Z., Zheng, H., Lucero, M., Wang, H., et al. (2020). Molecular engineering of dispersed nickel phthalocyanines on carbon nanotubes for selective CO2 reduction. Nat. Energy *5*, 684–692. https://doi.org/10.1038/s41560-020-0667-9.

36. Li, F., Li, Y.C., Wang, Z., Li, J., Nam, D.-H., Lum, Y., Luo, M., Wang, X., Ozden, A., Hung, S.-F., et al. (2020). Cooperative CO_2-to-ethanol conversion via enriched intermediates at molecule–metal catalyst interfaces. Nat. Catal. *3*, 75–82. https://doi.org/10.1038/s41929-019-0383-7.

37. Ozden, A., Li, F., García de Arquer, F.P., Rosas-Hernández, A., Thevenon, A., Wang, Y., Hung, S.-F., Wang, X., Chen, B., Li, J., et al. (2020). High-rate and efficient ethylene electrosynthesis using a catalyst/promoter/transport layer. ACS Energy Lett. *5*, 2811–2818. https://doi.org/10.1021/acsenergylett.0c01266.

38. Mardle, P., Cassegrain, S., Habibzadeh, F., Shi, Z., and Holdcroft, S. (2021). Carbonate ion crossover in zero-gap, KOH anolyte CO_2 electrolysis. J. Phys. Chem. C *125*, 25446–25454. https://doi.org/10.1021/acs.jpcc.1c08430.